PHYSICAL REVIEW B VOLUME 36, NUMBER 18 15 DECEMBER 1987-II

Quasielastic electron scattering as a probe of the silicon surface space-charge region

Joseph A. Stroscio* and W. Ho
Laboratory of Atomic and Solid State Physics and Materials Science Center, Cornell University, Ithaca, New York 14853
(Received 18 June 1987)

The quasielastic electron scattering from the Si(111)-7×7 surface is presented as a function of bulk impurity concentration, temperature, and oxygen exposure. The temperature dependence of the quasielastic peak is calculated for a given pinning position of the surface Fermi level and results observed on samples with different bulk impurity concentrations can be accounted for. From these measurements the temperature dependence of the surface depletion layer can be extracted. At high temperatures scattering from thermally activated free carriers in the conduction band is observed to give rise to a pronounced increase in the quasielastic peak width.

I. INTRODUCTION

A great deal of interest in the properties of semiconductor surfaces exists. Recent applications of electron energy-loss spectroscopy (EELS) has shown that quantitative information can be obtained concerning the transport properties of clean and metallized semiconductor surfaces.[1-5] The application of EELS to the study of the electronic properties of surfaces results from the interaction of the long-range Coulomb field of the incident electron with the surface excitations. In dipole scattering, the small momentum transfer at low loss energies allows EELS to probe the space-charge region of a semiconductor surface.[6] In the application of EELS to semiconductor surfaces two distinct regimes are usually encountered. At sufficiently high carrier densities well-resolved loss features due to surface plasmons may be observed in the loss spectra, as shown by Matz and Lüth.[7] The sensitivity of the losses to band bending at the surface was studied by Matz and Lüth with adsorbates on GaAs(110),[7] and also by Dubois and Schwartz in determining the influence of sputtering and annealing on GaAs(110).[8]

At lower carrier concentrations well-defined plasmon losses are no longer observed but instead the losses give rise to a broadening of the quasielastic peak. Quasielastic scattering can also occur from intrinsic surface-state excitations as observed on the Si(111)-7×7 surface. The sensitivity of the surface-state excitations was first shown by Backes and Ibach,[9] where the broadening of the quasielastic peak was found to decrease with the presence of adsorbates. Persson and Demuth[10] showed further that the quasielastic peak was temperature dependent and could be quantitatively analyzed to give useful information on the transport properties of the surface. Recently, Stroscio and Ho[3] showed that conduction-band carriers can also give rise to quasielastic scattering, which can be analyzed to provide information on band bending and Fermi-level pinning at a semiconductor surface. In this work a very strong dependence was observed at high temperatures and attributed to thermal activation of free carriers. Recently, Dubois *et al.*[11] observed similar quasielastic scattering from GaAs(100) where the high-temperature scattering was due mainly to the temperature dependence of the surface potential barrier but influenced negligibly by the thermally activated free carriers.

In this paper we give a detailed account of the quasielastic scattering from the Si(111)-7×7, including the dependence on doping of the high-temperature quasielastic linewidths, and the effects of adsorbates. In a previous report[3] the temperature dependence of the surface potential was not included in the analysis of the quasielastic peak, which resulted in a lower activation energy for thermal generation of carriers than expected.[12] In this work we analyze the quasielastic scattering and include the temperature dependence of the surface potential. The temperature dependence of the quasielastic scattering can then be fit using a single parameter, which is the surface Fermi-level position. For the Si(111)-7×7 surface we find that the Fermi level is pinned 0.58 eV below the conduction-band edge. This value is in good agreement with photoemission results, which typically yield values in the range 0.45–0.55 eV.[13] At high temperatures the dominant contribution to the quasielastic scattering is found to be the thermal activation of free carriers.

II. EXPERIMENTAL ARRANGEMENT

The experiments were performed in an ion, turbomolecular, and titanium sublimation pumped ultrahigh-vacuum system with a base pressure of $\leq 4\times 10^{-11}$ Torr. The EELS spectrometer consists of a double-pass 127° cylindrical deflection monochromator and analyzer.[14] The electron-impact energy was 6.8 eV and the angle of incidence was 60° with respect to the crystal normal. All measurements were made in the specular direction with an 8±1 meV full width at half maximum (FWHM) overall spectrometer resolution. The coarser resolution of 8 meV, compared to 4-meV capability, was chosen to limit fluctuations in the spectrometer resolution to ±1 meV. The FWHM of the quasielastic peak was obtained with an accuracy of 0.1 meV by a least-squares fit to a Gaussian line shape. The sample temperature was regulated with a pulsed current temperature controller.[15] The EELS spectra were collected during cycles when the heating current was gated off. Multiple sweeps of the spectra were collected with a multichannel analyzer for signal averaging.

 ©1987 The American Physical Society

The samples were obtained from (111)-oriented Si wafers with n-type As impurity concentrations ranging from 6.6×10^{12} to 1.0×10^{19} cm^{-3}. The bulk carrier densities were determined by conventional resistivity measurements and agreed within $\sim5\%$ with those given by the supplier.[16] The samples were cleaned by repeated cycles of Ne-ion bombardment at 500 eV, oxidation, and annealing to 1125 K. Surface cleanliness was monitored by Auger spectroscopy and EELS, which showed Si-C contamination during the initial stages of cleaning. Clean surfaces produced well-ordered 7×7 low-energy electron diffraction (LEED) patterns.

III. THEORY

The theoretical formalism for quasielastic scattering from surfaces was developed by Persson and Demuth.[10,17] Here we describe the relevant parts of the theory used in our calculations of the quasielastic scattering. We consider a beam of monoenergetic electrons of energy E and angle of incidence θ measured from the crystal normal. In the dipole scattering theory, the single-scattering probability integrated over the finite analyzer solid angle of acceptance is given by

$$P_s(\omega)=\frac{2}{(e_0\pi)^2k^2\cos^2\theta}\frac{v}{\omega}\times\int_0^{Q_c}\frac{dQ_\parallel}{Q_\parallel}f(vQ_\parallel/\omega,\theta)\mathrm{Im}[g(Q_\parallel,\omega)]\ , \quad (1)$$

where $f(x,\theta)$, $x=vQ_\parallel/\omega$, is given by

$$f(x,\theta)=\frac{1}{x}\int_0^{2\pi}d\psi\left[1+\left[\frac{1/x}{\cos\theta}-\tan\theta\cos\psi\right]^2\right]^{-2}\ . \quad (2)$$

Here $v=\hbar k/m$ is the velocity of the incident electron, a_0 is the Bohr radius, Q_c is the maximum parallel wave-vector transfer allowed by the acceptance angle of the analyzer, and $\mathrm{Im}[g(Q_\parallel,\omega)]$ is the linear-response function which describes the energy absorption in the medium. For small loss energies all the inelastic lobe of the scattered electrons is contained within the analyzer acceptance angle and thus the upper limit of the integral in Eq. (1) can be taken to infinity. For the function $f(x,\theta)$ we use a similar approximation to that given by Persson and Demuth[10] for $\theta=60°$,

$$f(x,60°)=\frac{0.39x^3}{1-0.81x+0.20x^4}\ . \quad (3)$$

This functional form is observed to have the correct limiting behavior for $x\to\infty$ and $x\to0$.

Due to the very low energy of the excitations, the inelastic scattering starts at very large distances from the surface and, as a result, multiple-scattering events must be considered. With allowance for multiple-scattering events at finite temperature the probability for scattering an incident electron can be obtained from the single-scattering probability $P_s(\omega)$ as

$$P(\omega)=\frac{1}{2\pi}\int dt\, e^{-i\omega t}\exp\left[\int d\omega'\,P_s(\omega')\{[n(\omega')+1](e^{i\omega' t}-1)+n(\omega')(e^{-i\omega' t}-1)\}\right]\ , \quad (4)$$

where $n(\omega)$ is the Bose-Einstein distribution function. The width of the quasielastic peak may be expressed in terms of the single-scattering probability without ever calculating the full multiple-scattering probability in Eq. (4) by considering the second moment,

$$\langle(\Delta\omega)^2\rangle=\langle(\omega-\langle\omega\rangle)^2\rangle\ , \quad (5)$$

where

$$\langle\omega\rangle=\int d\omega\,\omega P(\omega)\ .$$

Using Eq. (5), the width of the quasielastic peak may be obtained from $P_s(\omega)$ as

$$\langle(\Delta\omega)^2\rangle=\int d\omega\,\omega^2 n(\omega)P_s(\omega)\ . \quad (6)$$

Assuming a Gaussian line shape of the quasielastic peak (which is observed experimentally), the FWHM of the quasielastic peak is then given by $\Gamma^2=8\ln2\langle(\Delta\omega)^2\rangle$. Recently, Dubois *et al.*[11] showed that a simpler expression may be obtained for Γ by approximating the Bose-Einstein factor in Eq. (6). Equations (1) and (6) can be integrated numerically to obtain Γ, which is the method used in the present calculations.

A description of the substrate is contained in the response function Im(g). For a semi-infinite medium the response function is related to the dielectric function of the medium $\epsilon(Q_\parallel,\omega)$ as

$$\mathrm{Im}[g(Q_\parallel,\omega)]=\mathrm{Im}\left[\frac{-2}{1+\epsilon(Q_\parallel,\omega)}\right]\ . \quad (7)$$

For silicon we can describe the intraband excitations in the conduction band by a dielectric function,[18]

$$\epsilon(\omega)=\epsilon_0-\frac{\omega_p^2}{\omega(\omega+i/\tau)}\ , \quad (8)$$

where $\epsilon_0=11.7$ is the contribution from interband transitions and the plasmon frequency $\omega_p=(4\pi ne^2/m^*)^{1/2}$. The relaxation time τ can be related to the effective mass m^* and the mobility μ as $\tau=\mu m^*/e$. For silicon the effective mass $m^*=0.26m_e$ and the mobility $\mu\sim1200$ cm^2/V sec at carrier densities of $n=1\times10^{16}$ cm^{-3}.[19]

The dielectric function in Eq. (8) yields a scattering probability which is peaked at the surface plasmon frequency $\omega_{\mathrm{SP}}=\omega_p/(\epsilon_0+1)^{1/2}$ for $\omega_{\mathrm{SP}}\tau>1$, as shown in Fig. 1. For silicon we observe that at carrier densities below $\sim10^{17}$ cm^{-3} the plasmon frequency is comparable to the relaxation rate τ^{-1} and the loss structure becomes

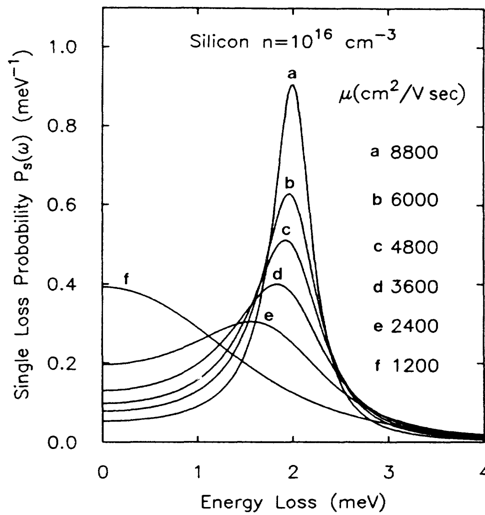

FIG. 1. Single loss probability for free-carrier excitations in silicon with a carrier density $n=10^{16}$ cm^{-3} as a function of mobility μ, ranging from 1200 to 8800 cm^2/V sec (for Si, $\mu=1200$ cm^2/V sec). The electron impact energy equals 6.8 eV and the angle of incidence equals 60°.

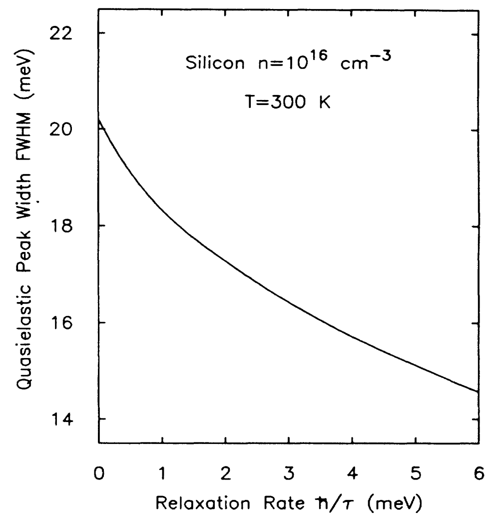

FIG. 2. The dependence of the relaxation rate on the quasielastic peak width for silicon with a carrier density of $n=10^{16}$ cm^{-3} at 300 K.

broad and featureless. The scattering probability as a function of mobility ranging from 1200 cm^2/V sec, which is characteristic of silicon,[19] to $\mu=8800$ cm^2/V sec, which is characteristic of GaAs,[20] is shown in Fig. 1. We see that for GaAs well-defined losses are predicted and have been observed by Matz and Lüth[7] (the smaller effective mass for GaAs also shifts the losses to higher energies). In contrast, for silicon the scattering probability is broad and featureless and should lead instead to a broadening of the quasielastic peak. However, at higher densities where the plasmon loss energies are sufficiently high, the loss structure should become observable outside the quasielastic peak, since $\omega_{SP}\tau>1$ for silicon with carrier densities greater than 10^{18} cm^{-3}.

The dependence of the relaxation rate on the quasielastic peak width, obtained from Eq. (6), is shown in Fig. 2. As expected from the dependence observed in the scattering probability, the quasielastic peak width decreases with increased relaxation rate τ^{-1}. For $\tau^{-1}>\omega_{SP}$ ($\omega_{SP}=2$ meV for $n=1\times10^{16}$ cm^{-3}) the rate of decrease is not significant and hence the temperature dependence of the mobility gives a negligible contribution to the temperature dependence of the quasielastic peak.

The temperature dependence of the quasielastic peak is discussed in the next section. We point out here that the approximate temperature dependence may be obtained by taking the $\tau\rightarrow\infty$ limit in Eq. (7), where one then finds the quasielastic peak width $\Gamma\propto\sqrt{T}$. Thus at sufficient low enough temperatures the quasielastic peak will be very small in comparison to the instrumental resolution, and the latter will dominate the measured linewidth of the quasielastic peak. An extrapolation to low temperatures may thus be used as a measure of the contribution of the spectrometer resolution. The temperature dependence which is observed in the calculated quasielastic peak is discussed in Sec. IV.

The magnitude of the quasielastic peak width as a function of carrier density is shown in Fig. 3. A substantial peak width of 10–30 meV, which is much larger than the instrumental resolution of $\sim$4 meV, may be obtained at nominal carrier densities. This explains why the EELS resolution observed on semiconductors is typically much poorer than on metal surfaces. The origin of the broadening of the quasielastic peak on semiconductors has previously been attributed to various other mechanisms such as work-function inhomogeneities or surface roughness.[21] However, we observe that the broadening can easily be explained by the strong multiple scattering of the incident electrons with very-low-

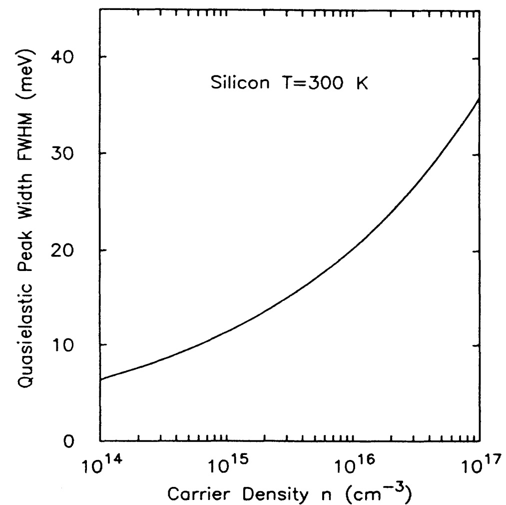

FIG. 3. The dependence of the quasielastic peak width on the carrier density for silicon at $T=300$ K.

energy electronic excitations, as observed in the experimental results shown below.

IV. RESULTS

A. Quasielastic scattering from Si(111)-7×7

The quasielastic peak for the Si(111)-7×7 surface is shown in Fig. 4 for various impurity concentrations. The sample temperature is 300 K. The silicon samples show a measurable broadening of the quasielastic peak in comparison to the instrumentally limited resolution observed on nickel (dashed line). In particular, the quasielastic peak shows an increase in width as the conduction-band carrier density increases. The quasielastic linewidth varies from 14 to 20 meV for the range of carrier densities shown in Fig. 4.

Figure 5 shows the quasielastic peak for a wider range of carrier densities. The increase in linewidth at intermediate carrier densities is followed by a decrease in the quasielastic peak at higher densities. Concomitant with this decrease is the appearance of a significant amount of loss intensity in the 20–30-meV region. This behavior is expected based on the discussion of the plasmon loss structure for silicon in the last section, where the plasmon loss moves outside the quasielastic peak at high enough carrier densities. The asymmetry observed between the loss and gain regions for the high-density sample is due to the Bose-Einstein occupation statistics, where the loss intensity is proportional to $n(\omega)+1$ and the gain intensity is proportional to $n(\omega)$.

The temperature dependence of the quasielastic peak is summarized in Figs. 6–8 for various impurity concentrations. The peak shape remains Gaussian up to temperatures approaching 1000 K.[3] A comparison is shown for similar measurements taken on a Ni(110) surface at the same spectrometer settings. A significant temperature dependence of the quasielastic peak is observed for Si, in contrast to Ni where no temperature dependence is observed. For a fixed temperature an increase in the

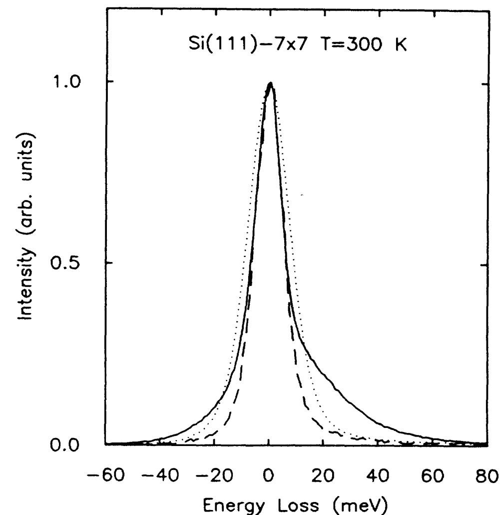

FIG. 5. A comparison of the quasielastic peak around the zero-energy-loss region from the Si(111)-7×7 surface with high, 4.5×10^{18} cm^{-3} (solid line); intermediate, 5.6×10^{16} cm^{-3} (dotted line); and low, 6.6×10^{12} cm^{-3} (dashed line), bulk impurity densities.

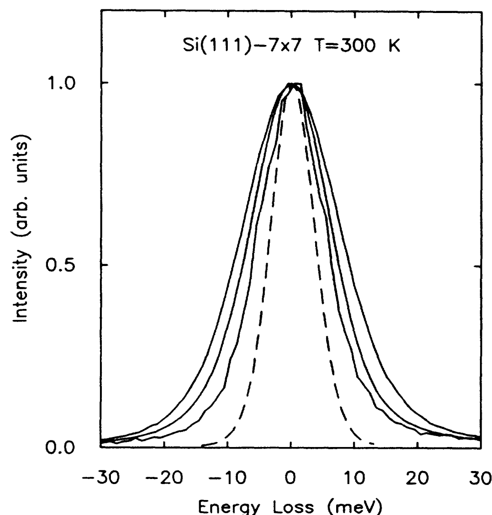

FIG. 4. The measured quasielastic peak around the zero-energy-loss region from the Si(111)-7×7 surface. The solid lines are the measured linewidths for three different samples with the following impurity densities: 6.6×10^{12}, 8.9×10^{15}, and 5.6×10^{16} cm^{-3}. The linewidth increases with increasing carrier density. The dashed line is a similar measurement from a clean Ni(110) surface obtained with the same spectrometer resolution.

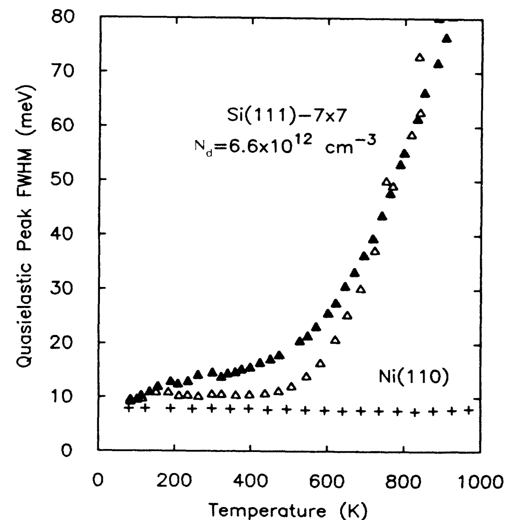

FIG. 6. Temperature dependence of the quasielastic peak width on the Si(111)-7×7 surface with bulk impurity concentration of $N_d=6.6\times10^{12}$ cm^{-3}: clean surface (solid triangle), surface exposed to 1 L O_2 (1 L$=10^{-6}$ Torr sec) at 80 K (open triangle). Temperature dependence of the quasielastic peak from a clean Ni(110) surface (crosses) is shown for comparison.

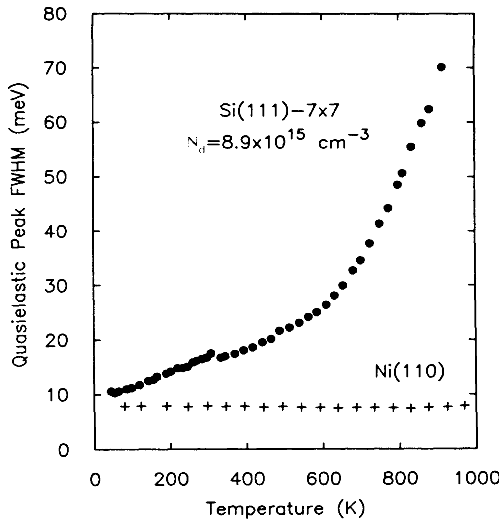

FIG. 7. Temperature dependence of the quasielastic peak width on the Si(111)-7×7 surface with bulk impurity concentration of $N_d = 8.9 \times 10^{15}$ cm^{-3}: clean Si(111)-7×7 surface (solid circle). Temperature dependence of the quasielastic peak from a clean Ni(110) surface (crosses) is shown for comparison.

quasielastic peak width is observed for increased impurity concentrations, similar to that observed in Fig. 4. Also shown in Figs. 6 and 8 is the effect of oxygen adsorption on the quasielastic peak width. For the nearly intrinsic sample in Fig. 6, the peak width is virtually diminished at low temperatures to that given by the instrumental resolution. For the higher doped sample in Fig. 8, the effect of the oxygen is to decrease the quasielastic peak width, but with a finite-temperature-dependent linewidth broadening which persists above the instrumental resolution.

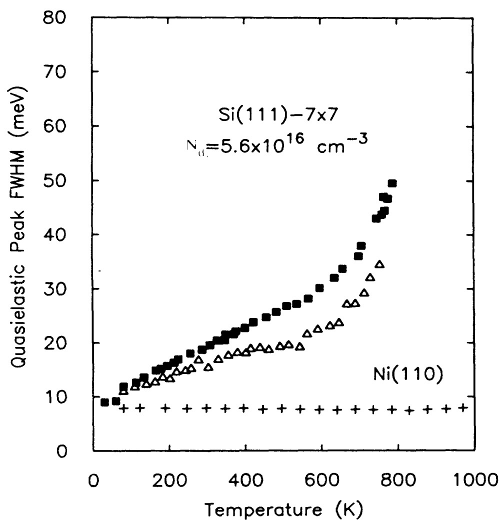

FIG. 8. Temperature dependence of the quasielastic peak width on the Si(111)-7×7 surface with bulk impurity concentration of $N_d = 5.6 \times 10^{16}$ cm^{-3}: clean surface (solid squares), exposed to 1 L O_2 at 80 K (open triangles). Results from a clean Ni(110) surface (crosses) are shown for comparison.

B. Depletion-layer model

An understanding of the quasielastic scattering from the Si(111)-7×7 surface must include the inhomogeneous carrier density in the surface region due to band bending. The presence of the high density of surface states in the band gap for the Si(111)-7×7 pins the Fermi level at approximately $\phi = 0.5$ eV below the conduction-band edge.[13] The resulting band bending and carrier concentration in the near-surface region, which is schematically shown in Fig. 9, can then be obtained from a solution of Poisson's equation with the appropriate boundary conditions.[22] For large surface barriers, a solution to Poisson's equation yields a depletion width given approximately by

$$d = \left[\frac{\epsilon_0 V_s}{2\pi n e} \right]^{1/2}, \tag{9}$$

where V_s is the magnitude of the surface barrier potential shown in Fig. 9. Within this approximation we can simulate the semiconductor surface using a three-layer model composed of vacuum, depletion layer, and substrate. The depletion layer is taken as a uniform slab of thickness d and dielectric constant $\epsilon_s = \epsilon_0$ on top of a substrate with dielectric constant ϵ_b given by Eq. (8). The effective dielectric function for this three-layer model is given by[6,23]

$$\epsilon(Q_\parallel, \omega) = \epsilon_s \left[\frac{1 + \Delta \exp(-2Q_\parallel d)}{1 - \Delta \exp(-2Q_\parallel d)} \right], \tag{10}$$

where $\Delta = (\epsilon_b - \epsilon_s)/(\epsilon_b + \epsilon_s)$. Equation (10) can then be used to obtain the response function in Eq. (7) and the

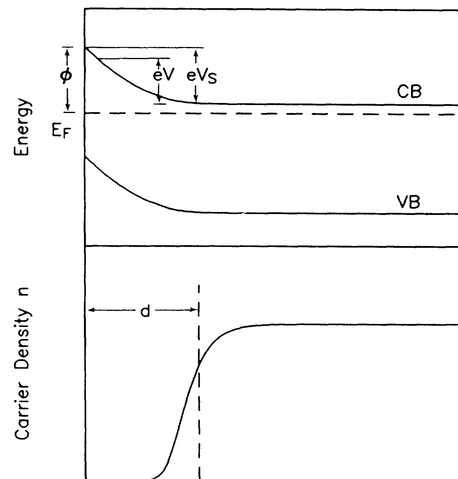

FIG. 9. Schematic diagram of band bending at a semiconductor surface and the resulting conduction-band carrier density normal to the surface.

width of the quasielastic peak via Eqs. (1) and (6). The above approximation treats the carrier density as changing abruptly in the depletion layer. More sophisticated calculations have been made for the varying carrier density profile and single-scattering loss functions at semiconductor surfaces.[24] The three-layer model is used here for its simplicity in describing the essential physics of the semiconductor surface and the ease with which it can be incorporated in the multiple-scattering theory. As shown below, this model successfully accounts for the scattering from depletion layers on n-type silicon surfaces.

For the Si(111)-7×7 there are two contributions to the quasielastic peak, as is evident from the scattering observed on the nearly intrinsic material shown in Fig. 6. In this case, the quasielastic peak broadening has been attributed to excitations within the metallic surface-state band on the Si(111)-7×7 surface.[1,10] This reasoning follows from the sensitivity of the scattering to very low coverages of adsorbates. For the present discussion we treat this as a background in our measurements and take the loss function as a sum of two terms given by

$$\mathrm{Im}g = \mathrm{Im}(g)_{\text{surface state}} + \mathrm{Im}(g)_{\text{conduction band}} \ . \tag{11}$$

This separation is in agreement with the observed behavior of the quasielastic peak with exposure to oxygen (see Figs. 6 and 8) which is discussed below.

The temperature-dependent broadening given by the first term in Eq. (11) has been previously described by Persson and Demuth.[10] This is fit to the low-temperature data for the intrinsic clean sample, as in Fig. 6. A value for the fitting parameter $\beta = 0.07$ meV (Ref. 25) is obtained, which is shown by the dashed line in Fig. 10. To describe the larger linewidths on the higher doped samples we consider the additional contribution due to excitation of free carriers in the conduction band. We may take as an unknown parameter the depletion width d and compare the measured linewidth with the calculated quasielastic peak width as a function of d, as shown in Fig. 11. The dashed curve in Fig. 11 shows the peak width due to conduction-band excitations. We observe that the peak width decays exponentially with a decay length which is inversely proportional to the surface-plasmon frequency.[3,12] The solid line has the added surface state and instrumental broadening convoluted in, which can be compared with experiment. From Fig. 11, we obtain a depletion-layer thickness of 1050 Å for the 5.6×10^{16} cm^{-3} impurity-doped sample. A similar calculation is shown in Fig. 12 for the 8.9×10^{15} cm^{-3} doped sample. The lower carrier density, and hence plasmon frequency, compared to the 5.6×10^{16} cm^{-3} sample yields a more slowly decaying peak width as a function of depletion-layer depth. A comparison with experiment gives a depletion depth of 1900 Å for this lower doped sample. These values compare favorably with the values estimated from Eq. (9) using the Fermi-level pinning deduced from photoemission. For example, with a pinning position at 0.53 eV below the conduction-band edge, Eq. (9) yields a depletion-layer thickness of 920 Å for a carrier concentration of 5.6×10^{16} cm^{-3}. Alternatively, one could use

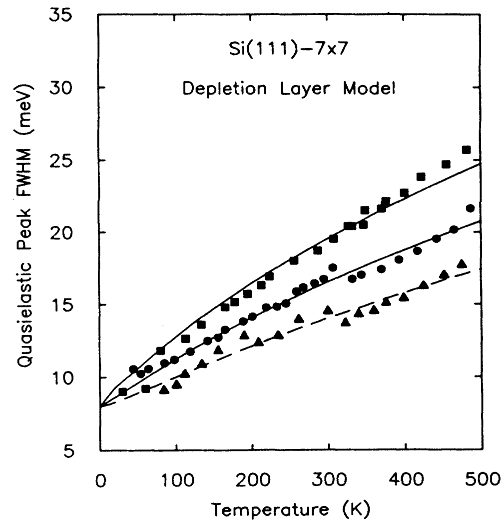

FIG. 10. A comparison of measured and calculated quasielastic peak width for the constant depletion-layer model. The measurements are for the bulk impurity concentrations of 6.6×10^{12} (solid triangle), 8.9×10^{15} (solid circle), and 5.6×10^{16} cm^{-3} (solid square). The dashed line shows the calculated linewidth due to surface-state excitations with $\beta = 0.07$ meV (Ref. 10). The upper two lines are obtained with the additional contribution from conduction-band carriers, with densities equal to the bulk values, and with depletion-layer depths of 1900 and 1050 Å, respectively.

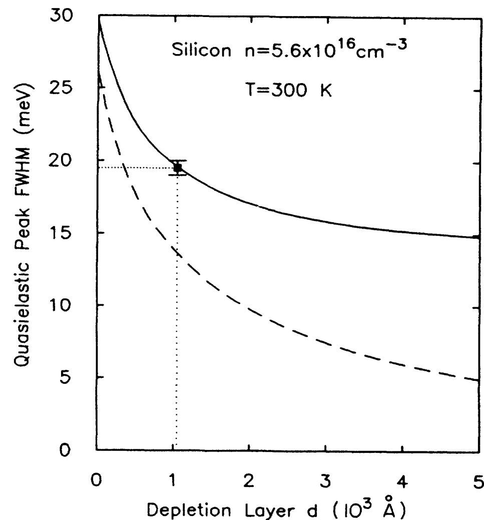

FIG. 11. The calculated quasielastic peak width as a function of depletion-layer thickness for $T = 300$ K and $n = 5.6 \times 10^{16}$ cm^{-3} (solid line) is due to contributions from the conduction band (dashed line), the surface state, and the 8-meV instrumental broadening. A comparison with the experimentally measured peak width (solid square) for $n = 5.6 \times 10^{16}$ cm^{-3} yields a depletion-layer thickness of 1050 Å.

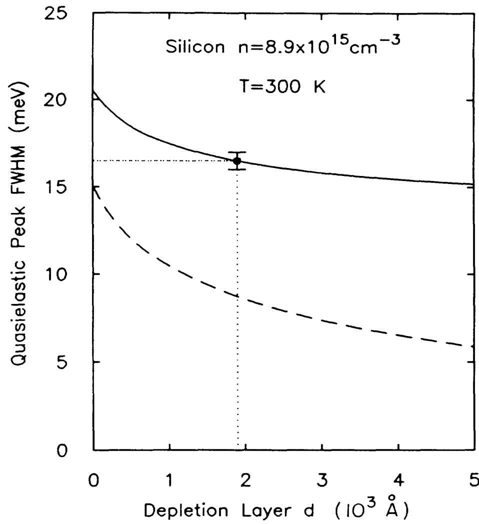

FIG. 12. The calculated quasielastic peak width as a function of depletion-layer thickness for $T=300$ K and $n=8.9\times10^{15}$ cm^{-3} (solid line) is due to contributions from the conduction band (dashed line), the surface state, and the 8-meV instrumental broadening. A comparison with the experimentally measured peak width (solid square) for $n=8.9\times10^{15}$ cm^{-3} yields a depletion-layer thickness of 1900 Å.

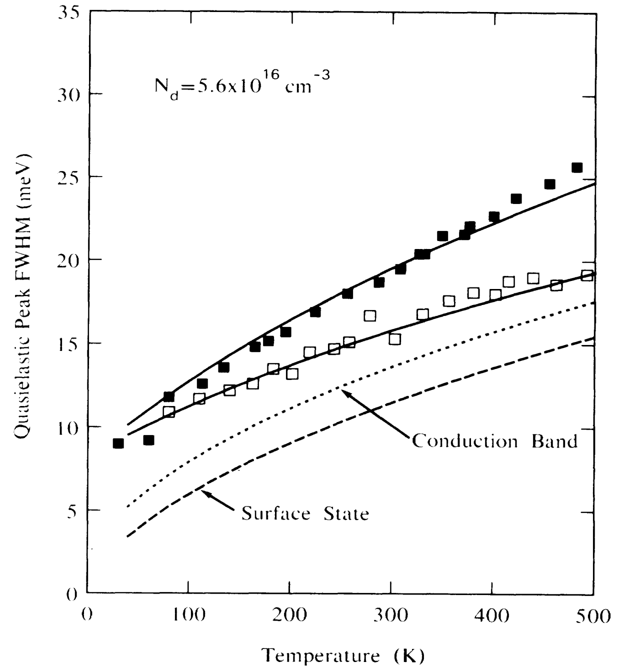

FIG. 13. A comparison of the measured and calculated temperature-dependent quasielastic peak width: clean surface (solid squares), surface exposed to 1 L O_2 at 80 K (open squares). The dashed line shows the width derived solely from the surface-state contribution while the dotted line shows the width solely from the conduction band. The upper solid line is obtained from combined contribution to the width from the surface state, conduction band, and instrumental resolution. The lower solid line through the open squares is the combined contribution from the conduction band and instrumental resolution.

the derived value of the depletion width to deduce the pinning position of the surface Fermi level.

The depletion-layer model can account for the full temperature dependence observed for the quasielastic peak. The various contributions to the temperature dependence of the quasielastic peak are shown in Fig. 13, assuming a temperature-independent depletion-layer thickness. For the range of temperature below ~400 K the observed temperature dependence of the quasielastic peak width for the clean surface (solid squares) is well accounted for. In addition, we show in Fig. 13 the contribution due solely to the conduction-band excitations, which fits the data observed on the oxygen-covered surface (open squares) well. The difference between the clean and oxygen-covered linewidths is the inclusion of the surface-state term for the clean surface data, which is derived from the measurements in Fig. 10. The separation of the loss functions in Eq. (11) is thus justified; the surface-state excitations are quenched with exposure to oxygen. The same effect is observed with minute amounts of hydrogen adsorption.[1]

Similar calculations for the temperature dependence of the quasielastic peak for the 8.9×10^{15} cm^{-3} sample is shown in Fig. 10, which summarizes results for the three samples. Deviation from the calculated linewidths in Fig. 10 can be observed for temperatures above 400 K, due to the assumption of a constant depletion-layer thickness. An examination of Eq. (9) shows this to be incorrect, as both the carrier density n and the surface barrier V_s are temperature dependent. We consider both these effects in the following section.

C. High-temperature behavior

The strong temperature dependence observed in the data in Figs. 6–8 is due to thermal generation of free carriers, as can be seen by examining the temperature dependence of the carrier density which is given by[26]

$$n(T)=\tfrac{1}{2}\{[(N_d-N_a)^2+4n_i^2]^{1/2}+(N_d-N_a)\}\ , \quad (12)$$

where N_d and N_a are the concentration of donor and acceptor impurities and where the intrinsic carrier density is

$$n_i(T)=[N_C(T)N_V(T)]^{1/2}e^{-E_g/2k_BT}\ , \quad (13)$$

where N_C and N_V are, respectively, the effective conduction- and valence-band densities of states which are proportional to $T^{3/2}$. The energy gap for silicon is given to linear order in T by[19]

$$E_g(T)=E_0-4.15\times10^{-4}T \quad (\text{eV})\ , \quad (14)$$

where $E_0=1.21$ eV. The linear coefficient in the gap energy thus changes the prefactor in Eq. (13) and the intrinsic carrier density is thus observed to follow the relation[19,27]

$$n_i(T)=3.73\times10^{16}T^{3/2}e^{-1.21\ \mathrm{eV}/2k_BT}\ \mathrm{cm}^{-3}\ . \quad (15)$$

Figure 14 shows the carrier density given by Eq. (12) for various impurity concentrations in n-type silicon. At low temperatures the carrier density is simply equal to the density of impurities which are fully ionized. At sufficiently low temperatures carrier freeze-out will occur where the density decreases below the impurity concentration, which is not shown in Fig. 14 (this occurs below $\sim$80 K for 10^{16} cm^{-3}). The transition between the extrinsic and intrinsic behavior at low and high temperatures is clearly seen in Fig. 14. With increased impurity concentration the transition to intrinsic behavior occurs at progressively higher temperatures. Precisely the same behavior is observed in the quasielastic peak width, shown in Figs. 6–8, where the rapid increase in width occurs at progressively higher temperatures with increasing impurity concentrations. Our previous analysis[3] demonstrated that this behavior could be accounted for by a temperature-dependent carrier density given by Eq. (12) with, however, a lower activation energy of 1.07 eV compared to the expected 1.21 eV, as indicated in Eq. (15).

An additional factor to consider in acccunting for the high-temperature behavior is the decrease in the surface potential V_s due to the shift of the bulk Fermi level to midgap as the temperature increases.[12] The position of the Fermi level (more correctly the chemical potential) is determined by the equilibrium carrier statistics and is given by[26]

$$\frac{N_d-N_a}{n_i}=2\sinh[\beta(E_F-E_{Fi})]\ , \quad (16)$$

where E_{Fi} is the intrinsic Fermi level taken to be midgap in the bulk. The surface potential V_s in Eq. (9) can be determined from the position of the bulk Fermi level E_F and the pinning position ϕ at the surface from the relation $eV_s=\phi-(E_c-E_F)$ (see Fig. 9). The temperature dependence of V_s thus results from the temperature dependence of the Fermi level. The pinning position ϕ is weakly temperature dependent due to the decrease in the band gap with increasing temperature.[11] The full temperature dependence of the surface potential is used to account for the temperature dependence of the quasielastic scattering, as shown below.

The pinning position at the surface can be extracted from the temperature dependence of the depletion layer, which can be obtained for each measured quasielastic peak width at a given temperature, as described in Sec. IV B. The full temperature dependence of the carrier density [Eqs. (12)–(14)] is included to give the correct dielectric function in Eq. (8). Figure 15 shows the temperature dependence of the depletion layer obtained by this method for the clean surface data shown in Fig. 7. A fit to the deduced temperature dependence of the depletion layer can be obtained from Eq. (9), including the temperature dependence of the surface potential V_s and the carrier density n. A best fit to the results in Fig. 15 is obtained with a pinning position of 0.58 eV below the conduction-band edge at 300 K, and is shown by the solid line. The temperature dependence of the surface potential is observed to give rise to the initial decrease in the depletion layer with temperature, whereas the tem-

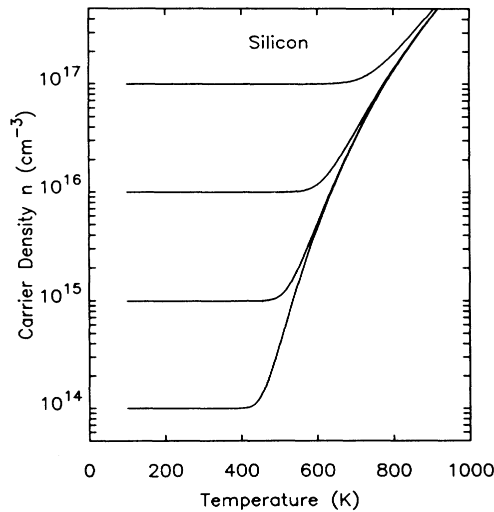

FIG. 14. The conduction-band carrier density [given by Eq. (12)] as a function of temperature and various impurity concentrations, 10^{14}, 10^{15}, 10^{16}, and 10^{17} cm^{-3}.

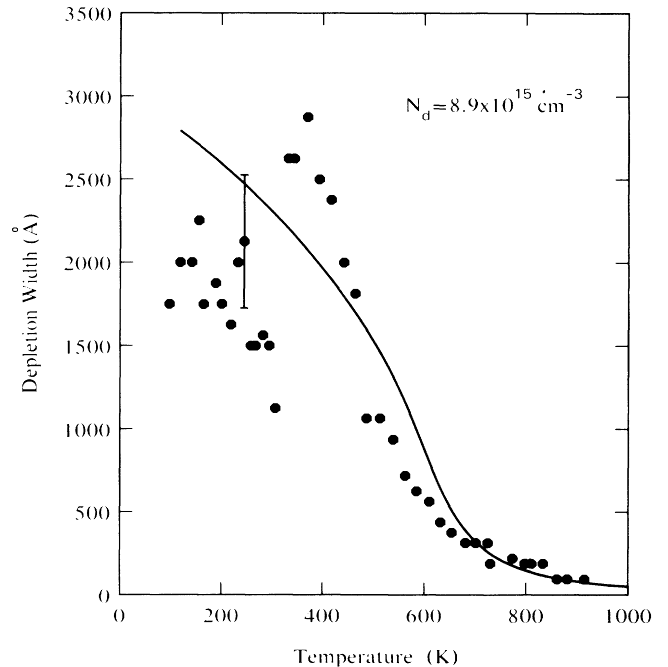

FIG. 15. Temperature dependence of the depletion-layer width, as deduced from the quasielastic peak width shown in Fig. 7 (solid circles), and calculated from Eq. (9) with a temperature-dependent carrier density and surface potential obtained from Eqs. (12) and (16) (solid line). The surface Fermi-level position is pinned at 0.58 eV below the conduction-band edge at 300 K. The error bar in the depletion width is due to an uncertainty of ±1 meV in the quasielastic width.

perature dependence of the carrier density causes the decrease in d for temperatures above 600 K. The success of the previous fit to the data in Fig. 10, assuming a constant d at low temperatures, is due to the finite contribution from the spectrometer resolution which limits the accuracy to which the linewidths can be measured. This can be seen by the scatter in the results in Fig. 15 at low temperatures where the relative contribution of the instrumental resolution is the largest. This scatter results from the slow decay in linewidth versus depletion width discussed above (see Fig. 12). A ± 1 meV change in linewidth results in ± 800 Å change in depletion width at 300 K, as indicated in Fig. 15. An overall decrease in the depletion width is still apparent in the data in Fig. 15 and agrees with the expected temperature dependence of d.

The effect of various functional forms for the temperature dependence of the depletion width on the temperature dependence of the quasielastic peak width is shown in Fig. 16. The dashed line is the calculated result for a constant depletion width, which is the result shown in Fig. 10, and clearly does not agree with the data at high temperatures. The good agreement with the solid line is based on the fit obtained in Fig. 15, including a thermal activation of carriers given by Eqs. (12)–(14) and also the temperature dependence of the surface potential with a Fermi-level pinning position of 0.58 eV. The dash-dotted curve shows the result with the carriers thermally activated but with d constant, which also fails to account for the high-temperature data. Similarly, the dotted curve shows the result including the temperature dependence of d without thermal activation of carriers (i.e., only including the temperature dependence of V_s). Clearly, this does not account for the high-temperature behavior, and thermal activation of carriers is the dominant mechanism for the large linewidths observed at high temperatures. This is in contrast to the recent results observed on the GaAs(100) surface,[11] which is most likely due to the larger band gap in GaAs (1.4 eV), and thus higher temperatures, above 900 K, are necessary before thermal activation makes a dominant contribution to the quasielastic scattering.

The surface pinning position determined from the data in Fig. 7 should also account for the data observed on the higher doped sample in Fig. 8, since the pinning position should be relatively invariant with impurity concentration. Figure 17 shows a fit to the quasielastic scattering for the 5.6×10^{16} cm^{-3} sample, using the pinning position of 0.58 eV below the conduction-band edge. As shown in Fig. 17 the fit accounts for the observed data without any additional adjustment of the parameters in the calculation. The dashed line in Fig. 17 is calculated using a pinning position of 0.63 eV, which shows the sensitivity of the fit to the choice of pinning position ϕ.

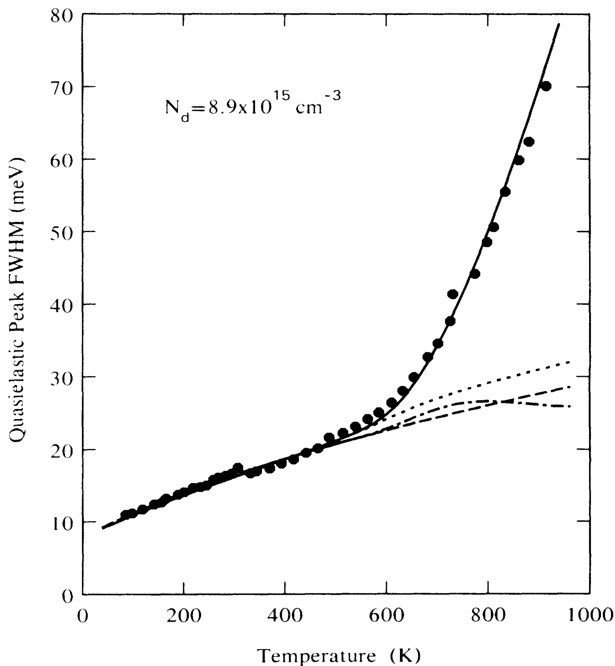

FIG. 16. A comparison of the measured quasielastic peak width with calculations for different temperature dependence of the depletion layer and carrier density. The data for the 8.9×10^{15} cm^{-3} impurity concentration is shown by the solid circles. Results for the calculations are for constant depletion layer and carrier density (dashed line), temperature-dependent carrier density and constant depletion layer (dot-dashed line), constant carrier density and temperature-dependent depletion layer (dotted line), and temperature-dependent carrier density and depletion layer given by the solid line in Fig. 15 (solid line). The Fermi-level pinning position $\phi=0.58$ eV.

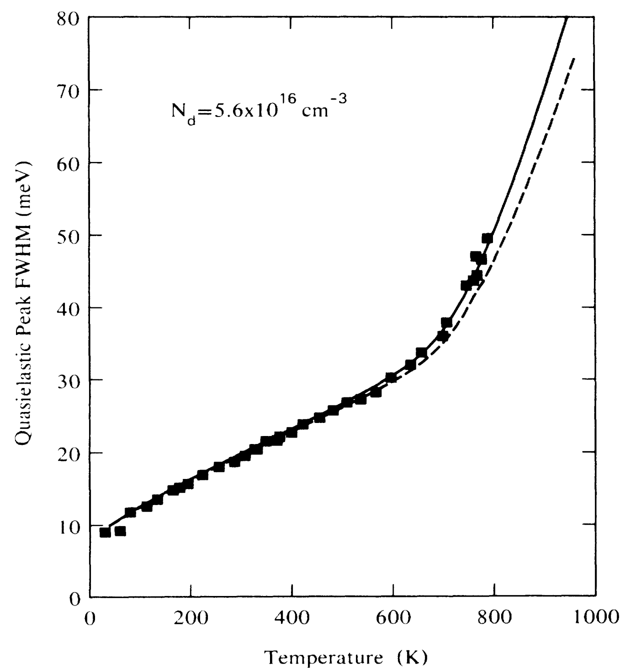

FIG. 17. A comparison of the temperature dependence of the measured quasielastic peak width (solid squares) and the calculated quasielastic peak width using the same pinning position $\phi=0.58$ eV (solid line) as deduced from Fig. 16. The dashed line shows the calculated quasielastic peak for $\phi=0.63$ eV. The impurity concentration is 5.6×10^{16} cm^{-3}.

In conclusion, we have shown that an analysis of the quasielastic scattering from the Si(111)-7×7 surface can yield information on the surface space-charge layer. We find that a pinning position of the surface Fermi level at 0.58 eV below the conduction-band edge can account for the observed temperature dependence of the quasielastic scattering on samples with various impurity concentrations. From measurement of the quasielastic peak the temperature dependence of the depletion layer at the surface can be extracted. The dramatic increase in the quasielastic peak width at high temperatures is found to be due to scattering from thermally activated free carriers in the conduction band.

ACKNOWLEDGMENT

Support of this research by the U. S. Office of Naval Research under Grant No. N00014-81-K-0505 is gratefully acknowledged.

---

[*]Present address: IBM Thomas J. Watson Research Center, Yorktown Heights, NY 10598.

[1]J. E. Demuth, B. N. J. Persson, and A. J. Schell-Sorokin, Phys. Rev. Lett. **51**, 2214 (1983).

[2]J. E. Demuth and B. N. J. Persson, Phys. Rev. Lett. **54**, 584 (1985).

[3]J. A. Stroscio and W. Ho, Phys. Rev. Lett. **54**, 1573 (1985).

[4]U. Backes and H. Ibach, Solid State Commun. **48**, 445 (1983).

[5]L. H. Dubois, G. P. Schwartz, R. E. Camley, and D. L. Mills, Phys. Rev. B **29**, 3208 (1984).

[6]See, for example, H. Ibach and D. L. Mills, *Electron Energy Loss Spectroscopy and Surface Vibrations* (Academic, New York, 1982).

[7]R. Matz and H. Lüth, Phys. Rev. Lett. **46**, 500 (1981).

[8]L. H. Dubois and G. P. Schwartz, J. Vac. Sci. Technol. B **2**, 11 (1984).

[9]U. Backes and H. Ibach, Solid State Commun. **40**, 575 (1981).

[10]B. N. J. Persson and J. E. Demuth, Phys. Rev. B **30**, 5968 (1984).

[11]L. H. Dubois, B. R. Zegarski, and B. N. J. Persson, Phys. Rev. B **35**, 9128 (1987).

[12]J. A. Stroscio, Ph.D. thesis, Cornell University, 1986.

[13]F. J. Himpsel, Th. Fauster, and G. Hollinger, Surf. Sci. **132**, 22 (1983); F. J. Himpsel, G. Hollinger, and R. A. Pollak, Phys. Rev. B **28**, 7014 (1983).

[14]J. A. Stroscio and W. Ho, Rev. Sci. Instrum. **57**, 1483 (1986).

[15]J. A. Stroscio, L. J. Richter, and W. Ho, Rev. Sci. Instrum. **55**, 732 (1984).

[16]The Si wafers were supplied by R. Tung of AT&T Bell Laboratories.

[17]B. N. J. Persson and J. E. Demuth, Phys. Rev. B **31**, 1856 (1985).

[18]See, for example, D. Pines, *Elementary Excitations in Solids* (Benjamin, New York, 1963), Chap. 4.

[19]H. F. Wolfe, *Silicon Semiconductor Data* (Pergamon, New York, 1969).

[20]C. Hilsum, *Semiconductors and Semimetals,* edited by R. K. Willardson and A. C. Beer (Academic, New York, 1966), Vol. 1, p. 16.

[21]H. Lüth, Festkorperprobleme **21**, 117 (1981).

[22]A. Many, Y. Goldstein, and N. B. Grover, *Semiconductor Surfaces* (North-Holland, Amsterdam, 1965), p. 136.

[23]D. L. Mills, Surf. Sci. **48**, 59 (1975).

[24]D. H. Ehlers and D. L. Mills, Phys. Rev. B **34**, 3939 (1986); **36**, 1051 (1987).

[25]The value of 0.07 meV deduced for β is slightly lower than the value of 1.1 meV deduced previously in Ref. 1. This could possibly be due to a contribution of the conduction-band excitations to the quasielastic peak in the data of Ref. 1.

[26]N. W. Ashcroft and N. D. Mermin, *Solid State Physics* (Holt, Rinehart and Winston, New York, 1976), p. 651.

[27]F. J. Morin and J. P. Maita, Phys. Rev. **96**, 28 (1954).